NASA TECHNICAL MEMORANDUM

NASA TM X-3289

NASA TM X-3289

COLD-AIR INVESTIGATION OF A 3½-STAGE FAN-DRIVE TURBINE WITH A STAGE LOADING FACTOR OF 4 DESIGNED FOR AN INTEGRAL LIFT ENGINE

I - Turbine Design and Performance of First Stage

Warren J. Whitney, Harold J. Schum, and Frank P. Behning

Lewis Research Center
Cleveland, Ohio 44135

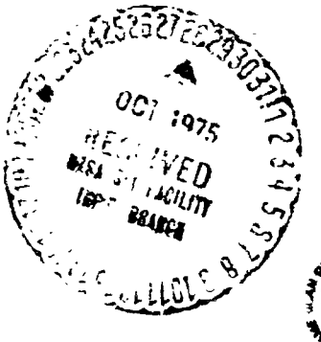

NATIONAL AERONAUTICS AND SPACE ADMINISTRATION • WASHINGTON, D. C. • OCTOBER 1975

COLD-AIR INVESTIGATION OF A 3½-STAGE FAN-DRIVE TURBINE WITH A STAGE LOADING FACTOR OF 4 DESIGNED FOR AN INTEGRAL LIFT ENGINE

I - TURBINE DESIGN AND PERFORMANCE OF FIRST STAGE

by Warren J. Whitney, Harold J. Schum, and Frank P. Behning

Lewis Research Center

SUMMARY

The procedure for designing a $3\frac{1}{2}$-stage turbine to drive the fan of an integral lift engine is presented. The conditions imposed by the engine result in a turbine with low blade speed, high stage loading factor, a moderately high specific-mass-flow requirement, and an outlet radius ratio of 0.5.

The first stage of the fan-drive turbine (which was initially designed to accommodate the flow conditions out of the high-pressure turbine) was modified to operate with axial inlet conditions by removing the prewhirl vanes and cutting back the leading edge of the stator blades. This stage was investigated as a single-stage turbine in cold air. The highest efficiency obtained at the design stage loading factor was 0.87, which was indicated at 116 percent of design speed and a total-pressure ratio of 1.415. This efficiency was 0.012 lower than that estimated by a reference prediction method. This result coincided closely with that obtained from a similar type single-stage reference turbine when compared at the same Reynolds number. The highest efficiency obtained for the turbine was 0.89 at 120 percent design speed and a total-pressure ratio of 1.27. A peak efficiency was not defined by the range of test conditions.

The efficiency at design specific work extraction and design speed was 0.358. The mass flow at this condition was 1.05 times the design value, and this excess mass flow indicated the desirability of a blading adjustment. It was determined from the velocity diagram that was constructed from the experimental data that the flow was underturned in the stator blade row and the rotor blade row by 1.4° and 1.7°, respectively.

INTRODUCTION

In recent years interest has increased in lift-fan engines for vertical and short takeoff and landing (VSTOL) aircraft. The NASA Lewis Research Center conducted a study to evolve the preliminary engine geometry and evaluate an integral lift engine for this type of application; the results are reported in reference 1. The physical features desired for this type of engine are compactness, lightweight, and a high ratio of thrust to engine and fuel weight. A requirement imposed on this engine by noise considerations is that the fan tip speed must not exceed approximately 305 meters per second (1000 ft/sec). The combination of this requirement and the engine geometry restrictions results in a fan-drive turbine that must develop its power at a relatively low blade speed. The fan-drive turbine must then be designed either with a few stages (e.g., $3\frac{1}{2}$) having a high stage loading factor (ratio of change in tangential velocity to blade speed) or with a large number of stages (e.g., 9 or 10) having conventional stage loading factors.

This report describes the design of a low-pressure (or fan-drive) turbine that was evolved for an integral lift engine. The aerodynamic design was performed to generate the blades for the three turbine stages, the inlet prewhirl vanes, and the outlet turning vanes. The turbine mechanical design was conducted, and the turbine blading and casing pieces were fabricated. The turbine was then modified to operate with axial inlet conditions to the first stage by removing the prewhirl vanes and cutting back the leading edge of the interstage stators. This modification was made in order to give the performance results a more general significance and to make them comparable with those obtained with other turbines designed with high stage loading factors. The modified first stage was then investigated in cold air as the initial phase of the turbine performance investigation. The nominal inlet conditions of pressure and temperature were 1.33 atmospheres and 378 K (680° R), respectively. The turbine was operated at 80, 90, 100, 110, and 120 percent of design speed over a wide range of total-pressure ratio (braketing design total-pressure ratio) at each speed. In addition to the turbine design procedure, this report presents the performance results obtained with the first stage.

SYMBOLS

A area, m^2; ft^2

C blade chord, cm

g force-mass conversion constant, 1; 32.174 ft/sec^2

h specific enthalpy, J/g; Btu/lb

l blade length, cm

N rotative speed, rpm

P absolute pressure, N/m^2; lb/ft^2

R gas constant for mixture of air and combustion products used in this investigation, 288 J/(kg)(K); 53.527 (ft-lb)/(lb)(^oR)

R_{stg} stage reaction, change in static enthalpy across rotor blade row divided by stage total enthalpy change; for first stage $R_{stg} = \left(W_{2,m}^2 - W_{1,m}^2\right) \Big/ 2\left(U\,\Delta V_{u,1-2}\right)_m$

R_x blade row reaction, change in kinetic energy across blade row normalized by outlet kinetic energy; for first-stage rotor $R_x = 1 - \left(W_1/W_2\right)_m^2$

r radius, cm

S blade spacing or pitch, cm

T temperature, K; ^oR

U blade velocity, m/sec; ft/sec

V absolute gas velocity, m/sec; ft/sec

W gas velocity relative to moving blade, m/sec; ft/sec

w mass-flow rate (sum of fuel and air), kg/sec; lb/sec

Z Zweifel loading coefficient; for first-stage rotor $Z = \left(2 \cos \beta_{2,m} \sin \Delta\beta_m \Big/ \cos \beta_{1,m}\right)\left(S/C_x\right)_m$

α absolute gas flow angle measured from axial direction, deg

$\overline{\alpha}$ average absolute gas flow angle at turbine outlet, measured as average deviation from axial direction irrespective of sign; used in eq. (?), deg

β relative gas flow angle measured from axial direction, deg

$\Delta\beta_m$ rotor blade turning angle

γ ratio of specific heats, 1.398 for mixture of air and combustion products used in this investigation

δ ratio of inlet total pressure to U.S. standard sea-level pressure

ϵ function of γ, $(0.73959/\gamma)\left[(\gamma + 1)/2\right]^{\gamma/(\gamma-1)}$

η_l efficiency based on total-pressure ratio

θ_{cr} squared ratio of critical velocity at turbine inlet to critical velocity of U.S. standard sea-level air

τ torque, N-m; ft-lb

Subscripts:

cr condition at Mach 1

h turbine hub section

m turbine mean section

t turbine tip section

u tangential component

x axial component

0 station at turbine inlet (see fig. 9(a))

1 station at stator outlet on velocity diagram

2 station at rotor outlet on velocity diagram

3 station at turbine outlet (see fig. 9(a))

Superscript:

' total state

TURBINE DESIGN

A candidate integral lift engine of 44 482-newton (10 000-lb) thrust was selected from a parametric computer-programmed study encompassing many engine cycle variations, component arrangements, and operational limitations. The computer program selected the number of turbine stages, determined a turbine component efficiency, and defined the turbine operational requirements, envelope geometry (maximum diameter and length), average stator outlet flow angle, and inlet and exit radius ratios. The subject turbine was designed to meet the operational requirements and to fit within or closely approximate the geometric limitations from the program.

Design Requirements

The requirements of the $3\frac{1}{2}$-stage fan-drive turbine at engine operating conditions are as follows:

Specific work, Δh, J/g; Btu/lb	180.16; 77.384
Mass flow, w, kg/sec; lb/sec	26.23; 57.83
Mean blade speed, U_m, m/sec; ft/sec	122.9; 403.1
Mean diameter (all stages), m; ft	0.498; 1.634
Inlet total temperature, T_0', K; $^\circ$R	1014.3; 1825.7
Inlet total pressure, p_0', atm	2.6104

The equivalent requirements for the same size turbine are as follows:

Equivalent specific work output, $\Delta h/\theta_{cr}$, J/g; Btu/lb	52.248; 22.445
Equivalent mass flow, $\epsilon w\sqrt{\theta_{cr}}/\delta$, kg/sec; lb/sec	19.128; 42.17
Equivalent mean blade speed, $U_m/\sqrt{\theta_{cr}}$, m/sec; ft/sec	66.17; 217.1

These requirements result in a low-speed turbine with a high stage loading factor (ratio of change in tangential velocity to blade speed, $\Delta V_t/U$) of approximately 4

The turbine geometry evolved in the design procedure was used in the mechanical layout and weight study of reference 1. The engine of reference 1 was scaled to increase the thrust to 1.25 times that of the candidate engine; therefore, all the turbine dimensions in reference 1 are 1.118 times those of the subject turbine.

Stage Work Split

An equal stage work split was considered desirable for the subject turbine for the following reasons: The inlet velocity diagram of the first stage is not significantly different from those of the second and third stages since it follows the high-pressure (HP) turbine in the engine. Also, there is no requirement for the third stage to operate with zero or limited exit whirl since it is followed by the outlet turning vanes. Finally, because the Mach number level in the turbine is low and the critical velocity does not change considerably from inlet to outlet, there is no reason to consider an equal equivalent work split, which is sometimes used to equalize Mach number among stages. Therefore, an equal stage work split was used, and the velocity diagrams at the mean radius were identical for the three stages.

Efficiency Estimation

The estimation of the efficiency of the turbine stages is an essential part of any design procedure. The working fluid total state determination at the various stations throughout the turbine is required to size the flow area properly. At the time this turbine was being designed there were no reliable experimental data on efficiencies of large aircraft turbines with high stage loading factors. Smith's curve (ref. 2, e.g.) shows no data above a stage loading factor of 2.4 and only a few points above 2.0. In the work of reference 3 a procedure was derived to predict the efficiencies of turbines that have high stage loading factors. This method consisted of determining each blade row loss as the product of an empirical loss coefficient and the average kinetic energy of the fluid relative to the blade row. The loss coefficient was obtained from performance results of turbines that had conventional stage loading factors (1 to 2). The estimated efficiency trends obtained from this procedure are shown in figure 1(a). The efficiency estimation procedure used in the design of the subject turbine was similar to that of reference 3 except that the loss coefficient was increased for conservative practice, which resulted in the efficiency trends shown in figure 1(b). The estimated stage efficiency used in the design was 0.819 (for all three stages), which resulted in an overall three-stage turbine efficiency of 0.829. The overall efficiency did not include the loss of the outlet turning vanes.

In addition to stage efficiency, the distribution of loss within the stage between stator and rotor components must be estimated. This was done by assuming that the fraction of total pressure lost in the stator blade row was equal to two-thirds of the fraction of relative total pressure lost in the rotor blade row. The corresponding total-pressure ratios for the stator and rotor blade rows were 0.9777 and 0.9665, respectively. This loss distribution assumption, which was based on past experience of correlating experimental and analytically predicted turbine performance data, was used to size the stator outlet flow area.

Velocity Diagrams

The velocity diagrams generated for the fan-drive turbine are shown in figure 2. The velocity diagram for the HP turbine is included in the figure since the HP turbine outlet conditions are the inlet conditions of the fan-drive turbine. The subscript 1 denotes the free-stream conditions at the stator outlet, and the subscript 2 those at the rotor outlet. The mean radius diagram is for a constant mean diameter, 0.498 meter (19.607 in.), while the hub and tip diagrams represent varying diameters. The hub and

tip diagrams are shown for the diameter corresponding to the blade outlet throat midpoint.

At the mean radius the velocity diagram closely approximates a symmetrical diagram, which is characterized by the relations $\left(W_2 = V_1\right)_m$ and $\left(\alpha_1 = -\beta_2\right)_m$. The stage reaction R_{stg} of the fan-drive turbine was increased slightly from that of a symmetrical diagram, so that $\left(V_{x,2} = 1.023\ V_{x,1}\right)_m$ and $\left(-W_{u,2} = 1.015\ V_{u,1}\right)_m$. The radial variation of the velocity diagram was determined from the free-vortex relations of constant axial velocity and absolute tangential velocity varying inversely with radius. The velocity diagram of the fan-drive turbine does not pose any particularly severe problems such as high relative Mach number or excessive blade turning. The reaction across the blade sections is reasonably high except in the first-stage stator tip section. The most unusual feature of the diagram is the low blade speed, or the high ratio of tangential velocity change to blade speed.

Blade Design

The objective of the blading design evolved to fit the velocity diagram of figure 2 was to obtain a lightweight turbine within the diameter and length allotted for this component. The blade rows, except for the first-stage (or interstage) stator, had average axial chords of 2.8 to 3.0 centimeters (1.1 to 1.2 in.) and resulting aspect ratios from 3.6 to 5.8. The first-stage stator was conceived as an engine frame (ref. 1) as well as a transitional stator and had longer chord airfoils. The number of blades was determined by selecting Zweifel loading coefficients (refs. 4 and 5) of 0.8 for the stators and 0.9 for the rotors. The stator blade axial chord was varied linearly with radius, and the result was a Zweifel loading coefficient that was nearly constant with radius for all three stator blade rows. A similar attempt to equalize the blade loading coefficient with radius for the rotor blading would have resulted in an inverse taper; that is, the largest axial chord would have occurred at the tip radius. Thus, a constant axial chord was used for all three rotor blade designs because of mechanical considerations.

The blade section stacking procedure is described in the section Blade Section Stacking. However, part of the stacking information must be known or assumed for the design procedure. First, the relative axial position of the three sections must be available to be used as input to the design procedure. Second, the blade must be essentially radial (without tangential lean) so that the assumption that the blade exerts no radial force on the fluid is valid.

The blade channels were laid out at constant radii at hub, mean, and tip sections. Curved suction surfaces were used upstream and downstream of the guided blade

channel. The blading inlet and outlet channel orthogonals were determined from the free-stream conditions by using continuity and constant angular momentum relations as discussed in reference 6. The blading channels had a conventional generally convergent area variation, as shown in figure 3 for two typical sections. The design method was quasi-three-dimensional and is described in references 6 and 7. The velocity distributions for the blading are shown in figure 4, and the blading passages and profiles are shown in figure 5. The flow path projection in the radial-axial plane is represented in figure 6, where the low radius ratio r_h/r_t at the turbine outlet (0.497) can be seen.

Prewhirl Vanes and Outlet Turning Vanes

The prewhirl vanes were required to simulate the flow conditions out of the HP turbine. The outlet turning vanes were necessary to convert the whirl velocity out of the third stage to axial velocity for useful thrust. Both sets of vanes were designed by using reference 8 as a guide. The outlet guide vanes were designed with a diffusion factor (ref. 8) of 0.4 at the mean radius. Double-circular-arc airfoils were used that had a circular-arc mean camber line and a maximum thickness of 0.095 of the camber line length. Carter's rule, as discussed in reference 8, was used for the deviation angle.

The prewhirl vanes were also double-circular-arc airfoils with a circular-arc mean camber line. The design procedure was similar to that for the outlet turning vanes, except that a Zweifel coefficient was used to select the solidity rather than a diffusion factor.

Blade Section Stacking

All the blading was defined by the section geometry at constant radii corresponding to the hub, mean, and tip diameters of the blade rows. The blade was formed by positioning the three sections and fairing a smooth surface through them. The stator blade, prewhirl vane, and outlet turning vane sections were positioned so that the centers of their trailing edge circles lay on a radial line. The rotor blade sections were positioned so that the line connecting their leading edges and the line connecting their trailing edges lay in planes that were perpendicular to the axis of rotation. The sections were adjusted tangentially to position their centroids in approximately the same radial-axial plane. Because of the low operating blade speed and low blade stress level, an outer shroud was incorporated into the rotor blade designs to minimize the blade row end losses. A number of features of the blading design are listed in table I. The stage

reaction R_{stg} for all three stages is 0.54. The blade section coordinates are listed in table II.

FIRST-STAGE MODIFICATION

The $3\frac{1}{2}$-stage turbine was initially conceived as a component of an integral-lift engine with prewhirl vanes to simulate flow conditions out of the HP turbine. While the turbine parts were being fabricated, two turbines were being investigated under contract (refs. 9 and 10). These contract investigations involved a three-stage turbine with an average stage loading factor of 3 (ref. 9) and a $4\frac{1}{2}$-stage turbine with an average stage loading factor of 5 (ref. 10). Both of the reference turbines had axial flow entering the turbine. It was therefore decided to modify the subject turbine for axial inlet conditions to make the results more comparable with those of the reference turbines and with those of future turbines with high stage loading factors. This procedure would eliminate the variable of inlet whirl from the performance comparison.

The first-stage stator was accordingly modified by cutting back the leading edge to such a degree that the mean camber line was oriented in an axial direction. The prewhirl vanes were removed, and the inlet duct was altered to provide a smoother area change between the turbine inlet and the stator blade leading edge (see fig. 7). This turbine inlet configuration is far from ideal since it is long and it diffuses the flow and is therefore conducive to boundary layer buildup. It was, however, considered expedient to modify the inlet in this manner rather than remachine the large turbine inlet casing. The flow path fairings that were provided for single-stage tests were installed at the turbine outlet. The flow path of the modified single-stage turbine configuration is shown in figure 7. The modified first-stage stator blade forms are shown in figure 8(a). The velocity diagram and blade surface velocity distributions for the modified blade are shown in figures 8(b) and (c), respectively. The modified first-stage stator geometry is presented in table II(i).

The efficiencies estimated in the design procedure for the initial turbine configuration were the following: stage efficiency, 0.819, and overall three-stage turbine efficiency, 0.829, as discussed previously. The estimated efficiency for the modified first stage was revised to 0.857 (fig. 1(b)), since it operated as a first stage rather than an intermediate stage. This change in estimated efficiency would require a small reduction in the blade row outlet areas for both the stator and rotor blade rows; however, the blade setting angles were not changed, since this would entail remachining the rotor assembly and the stator retaining rings. The equivalent performance requirements for the modified single-stage turbine were

Equivalent specific work output, $\Delta h/\theta_{cr}$, J/g; Btu/lb	17.416; 7.482
Equivalent mass flow, $\epsilon w\sqrt{\theta_{cr}}/\delta$, kg/sec; lb/sec	19.128; 42.17
Equivalent mean blade speed, U_m/θ_{cr}, m/sec; ft/sec	66.17; 217.1
Total-pressure ratio based on efficiency of 0.857	1.290

Some of the design features listed in table I for the first-stage stator blade were altered by the geometry modification. For the modified first-stage stator these features were the following:

Mean radius blade chord, C_m, cm	4.471
Mean radius solidity, C_m/S_m	1.572
Aspect ratio, ℓ/C_m	2.14
Zweifel loading factor	0.718
Reaction	0.656

APPARATUS, INSTRUMENTATION, AND PROCEDURE

The test facility was that described in reference 7. The modified single-stage turbine test section is shown in figure 9(a). The research instrumentation is represented in figure 9(b). The $3\frac{1}{2}$-stage turbine rotor assembly is shown in figure 10.

The type of research data and the data acquisition methods are essentially the same as those described in reference 7 and are reviewed briefly in this section. Airflow was measured with a calibrated Dall tube, which is a special type of venturi meter. Fuel flow to the turbine inlet-air heater was measured with a flat plate orifice. Both of these flow measurements required an upstream temperature, an upstream pressure, and a characteristic differential pressure, as specified by the flowmeter. The turbine mass-flow rate was determined as the sum of these two flows.

Turbine rotative speed was measured with an electronic counter that registered the impulses as the teeth on a sprocket mounted on the turbine shaft passed a stationary magnetic pickup. Turbine torque was measured as the reaction torque on the cradled dynamometer stator with a strain-gage load cell. The load cell and the digital voltmeter readout system were calibrated before and after each day's running.

The turbine was instrumented at three axial positions (fig. 9(a)). At the inlet to the stator (station 0) the instrumentation consisted of six wall static-pressure taps, one rake of five thermocouples, and two Kiel total-pressure probes, all located as shown in figure 9(b). Three static-pressure taps were installed on the inner walls and three on the outer walls in the circumferential locations shown in figure 9(b). The thermocouples were used with a recovery calibration to yield turbine inlet total temperature. The five

thermocouple sensing heads were located at the area center radii of five equal annular areas. The Kiel total-pressure probes were connected to mercury manometers in the control room; the manometers were used solely for setting and monitoring the desired turbine inlet total pressure during tests.

At station 1 (see fig. 9(a)), between the stator and the rotor, the static pressure was measured by three taps on the inner shroud and three on the outer shroud slightly downstream of the stator blade trailing edges and on the projected flow passage centerline. These pressure measurements were assumed to indicate the average stator outlet pressure at the hub and tip radii.

Turbine outlet conditions were measured at station 3 (fig. 9(a)), located $1\frac{1}{2}$ axial rotor blade chord lengths downstream of the rotor blades. The instrumentation included eight static-pressure taps and provisions for 10 flow-angle measurements. The eight taps were located with four on both the inner and the outer walls, each set being equally spaced circumferentially with the corresponding inner and outer taps at the same circumferential position (fig. 9(b)). The 10 turbine outlet flow-angle measurements were taken by using two actuators, each equipped with an angle-sensitive and self-alining probe. The circumferential positions of the actuator axes were $13\frac{1}{2}$ stator blade passages apart. For each test data point, then, the probes were traversed radially to the area center radii of five equal annular areas, and at each stop the indicated flow angles were recorded. The observed 10 readings were subsequently numerically averaged.

Each item of research data information was converted to electrical signal by an appropriate transducer and transmitted to a 100-channel data recording system. The recorded data and the necessary calibrations were then used as input to the computer program to obtain the performance parameters. In addition, all the pressures were recorded by photographing a mercury manometer board. Mass flow indicating data (temperature and pressures), torque, speed, and flow angle were also hand recorded for a number of selected data points at design speed. These points were then manually computed to verify the automatic data recording system and the computer program.

The turbine was operated at nominal inlet conditions of 1.33 atmospheres and 378 K (680° R). The speeds investigated were 80, 90, 100, 110, and 120 percent of design speed. At each speed data points were taken over a range of pressure ratios bracketing the design total-pressure ratio of 1.292.

The turbine efficiency was based on total-pressure ratio. The inlet total pressure was calculated by using static pressure, mass flow, and total temperature as follows:

$$\frac{p_0'}{p_0} = \left[\frac{1}{2} + \sqrt{\frac{1}{4} + \frac{\gamma - 1}{2g\gamma}\left(\frac{w}{p_0 A_0}\right)^2 RT_0'}\right]^{\gamma/(\gamma-1)} \tag{1}$$

The outlet total pressure was calculated similarly; however, since the flow is not axial at the outlet, the flow angle must be included in the equation:

$$\frac{p_3'}{p_3} = \left[\frac{1}{2} + \sqrt{\frac{1}{4} + \frac{\gamma - 1}{2g\gamma} \left(\frac{w}{p_3 A_3} \right)^2 \frac{RT_3'}{\cos^2 \bar{\alpha}}} \right]^{\gamma/(\gamma-1)} \tag{2}$$

The total temperature T_3' in equation (2) was determined from inlet total temperature, turbine torque, speed, and mass flow. The angle $\bar{\alpha}$ in equation (2) is the average deviation from the axial direction, irrespective of sign.

The data were faired to obtain the performance map in the following manner: The data for each of the three experimentally obtained parameters, equivalent torque, equivalent mass flow, and outlet flow angle, were first plotted as functions of inlet total- to outlet static-pressure ratio. Smooth curves were faired on these plots through the experimental data points for each speed. The performance map was then constructed by using the faired value of equivalent torque, equivalent mass flow, and outlet flow angle for the particular total- to static-pressure ratio and turbine speed.

RESULTS AND DISCUSSION

This section includes the overall single-stage turbine performance, a comparison with contemporary high-stage-loading-factor turbines, and a discussion of possible blading adjustments.

Overall Stage Performance

The experimental data are shown in figures 11 to 13 with equivalent torque $\epsilon\tau/\delta$, equivalent mass flow $\epsilon w\sqrt{\theta_{cr}}/\delta$, and outlet flow angle $\bar{\alpha}$ shown as functions of the total- to static-pressure ratio p_0'/p_3. Smooth curves were faired through the data points in these figures, and the faired quantities were used to construct the performance map, as discussed in the previous section. The maximum deviation from the faired curves is within 1/2 percent for torque (fig. 11) and within 1/4 percent for mass flow (fig. 12). The deviation in flow angle (fig. 13) is in most cases within $1/2^\circ$. The equivalent torque curves (fig. 11) indicate that the turbine did not approach limiting loading at any speed for the range of pressure ratio investigated. The fact that the

limiting-loading pressure ratio would be far removed from that corresponding to design work output would be anticipated for this design because of its low blade speed and low blade relative Mach number. Design specific work output occurred at a total- to static-pressure ratio of about 1.56 at design speed. The equivalent mass flow curves (fig. 12) show that the turbine choked at all speeds at the higher pressure ratios. The choking mass flow was dependent on rotor speed, which indicated that the choking occurred in the rotor blade.

The overall stage performance map constructed from the experimental data is shown in figure 14. The efficiency varied from a low value of 0.80, which occurred at 80 percent speed at a total-pressure ratio p'_0/p'_3 of 1.37, to a high value of 0.89, which occurred at 120 percent speed at a total-pressure ratio of 1.27. A maximum or peak efficiency was not defined at any of the pressure ratios. At design equivalent specific work output (17.416 J/g; 7.482 Btu/lb), the highest efficiency obtained was between 0.885 and 0.89. The first two points of interest to be discussed are denoted in figure 14 as A and B. Point A represents equivalent design specific work output at design speed, and point B represents equivalent design mass flow at design speed. The turbine equivalent design specific work output (point A) occurred at an efficiency of 0.858, which is very close to the revised estimated efficiency for the modified first stage, 0.857. The mass flow at design work extraction was 1.05 times the design value. This excess mass flow can be noted in figure 14 by comparing the abscissa values of points A and B. The excess mass flow occurring at design work extraction indicates the desirability of a blading geometry adjustment. The points C, D, and E are located in figure 14 at the specific work output values corresponding to the design stage loading factor at 90, 110, and 120 percent of design speed, respectively. The line connecting these points (and point A) represents operation at the design stage loading factor. At 90 percent speed (point C), the efficiency at the design stage loading factor was the same as that at design speed, 0.858. At 110 and 120 percent of design speed (points D and E), the turbine operated at the design stage loading factor with an efficiency between 0.865 and 0.87. The highest efficiency indicated at the design stage loading factor was 0.87, at approximately 116 percent of design speed at a total-pressure ratio of 1.415. The specific work output at this point was 1.34 times the design value.

In summary, the performance results indicate that the turbine achieved a maximum efficiency at the design stage loading factor of 0.87 at 116 percent of design speed. The efficiency at design speed and design work output was 0.858. The excessive mass flow (1.05 times design) at this condition indicates the desirability of a blading geometry adjustment.

Comparison of Performance of Fan-Drive Turbine and Contemporary High-Stage-Loading-Factor Turbines With Predicted Performance

As discussed in the section TURBINE DESIGN, at the time the turbine was designed there were no experimental data available for turbines operating with high stage loading factors from which to estimate efficiency. The estimating method used was based on extrapolation of loss coefficients obtained from turbines operating with conventional stage loading factors (below 2.0). Since the turbine was designed, however, experimental results for high-stage-loading-factor turbines have been reported in references 9 and 10. The performance levels from the reference turbines are cited for an inlet pressure of 1.33 atmospheres in order to compare the reference results with those of the subject turbine at approximately the same blade flow channel Reynolds number.

The turbine of reference 10 was a $4\frac{1}{2}$-stage turbine with an average stage loading factor of 5. This turbine achieved design work output at an efficiency of 0.845 at an inlet pressure of 1.33 atmospheres. The overall efficiency was estimated for this turbine by using the design stage loading factors (from ref. 10) and the estimated stage efficiencies (from ref. 3). This estimated overall efficiency, not including the outlet turning vane loss, was 0.847. The outlet turning vane loss in turn was calculated (by using ref. 8) to cause a decrease in overall efficiency of 0.004. When this loss is considered, the experimental performance is in close agreement with that predicted by using reference 3. The individual stage efficiencies, however, could not be determined from reference 10 because the investigation was limited to the one configuration, that of the complete $4\frac{1}{2}$-stage turbine.

The turbine of reference 9 was a three-stage turbine with an average stage loading factor of 3. The first stage of this turbine, which had a stage loading factor of 4.2, was tested as a single-stage turbine. This configuration developed design work output with an efficiency of 0.868 at an inlet pressure of 1.33 atmospheres. The efficiency estimated from reference 3 for this turbine stage was 0.879, or about 1 point higher (fig. 15). The reference turbine was also run at increased inlet pressure to determine the effect of Reynolds number on performance. The efficiency obtained at the highest inlet pressure (2.67 atm) is also shown in figure 15. This increase in Reynolds number effected an improvement in efficiency of slightly over 1 point, and the efficiency at the highest inlet pressure was very close to the predicted efficiency from reference 3.

The efficiency predicted from the reference 3 curve for the subject single-stage turbine was 0.882, or 1.2 points higher than the maximum (0.87) obtained at the design stage loading factor (fig. 15). This result coincides closely with that obtained for the similar type single-stage turbine of reference 9 at the inlet pressure of 1.33 atmo-

spheres. The subject turbine could not be operated at higher inlet pressure because of facility limitations.

Blading Adjustment

Velocity diagrams were constructed from the experimental data for points A and B on the performance map (fig. 14). In this procedure it was assumed that the average flow conditions could be represented by a single diagram at the mean radius. The experimental quantities used were equivalent mass flow, average outlet flow angle, equivalent specific work output, and total- to static-pressure ratio. The diagrams for points A and B are presented in figures 16(a) and (b), respectively, and are compared with the design mean radius diagram. The comparison indicates that underturning occurred in both blade rows. The stator outlet flow was underturned by 1.4° and that of the rotor by 1.7°. At the condition of design mass flow (fig. 16(b)) the velocity vectors are smaller than design because they are oriented too close to the axial direction and the necessary change in angular momentum of the flow is not developed. As the pressure ratio is increased to produce design specific work (fig. 16(a)), the axial velocity and the mass flow become too large. The conditions of design mass flow and design specific work could be made to coincide (or very nearly so) by making the indicated blade angle adjustments. It is felt that this would also cause the efficiency at design work output to increase since the peak efficiency region would tend to fall closer to the design point.

SUMMARY OF RESULTS

A $3\frac{1}{2}$-stage turbine with a stage loading factor of 4 was designed to drive the fan of an integral lift engine. The first stage of this turbine was investigated experimentally in cold air. The following results were obtained from the experimental investigation:

1. The highest efficiency obtained at the design stage loading factor was 0.87, which was indicated at 116 percent of design speed at a total-pressure ratio of 1.415. The corresponding specific work output was 1.34 times the design value.

2. The efficiency of 0.87 was 0.012 lower than that estimated from a reference prediction method. This result coincided closely with that obtained from a reference single-stage turbine of a similar type when the reference turbine was operated at approximately the same Reynolds number.

3. The turbine efficiency at design speed and design equivalent specific work output was 0.858. The excess mass flow at this condition (1.05 times design) indicated the desirability of a blading geometry adjustment.

4. The velocity diagram constructed from the experimental work output, outlet flow angle, mass flow, and total- to static-pressure ratio indicated that the flow was underturned in the stator blade row and the rotor blade row by 1.4° and 1.7°, respectively.

5. The highest efficiency obtained was 0.89, which occurred at 120 percent of design speed at a total-pressure ratio of 1.27. A maximum or peak efficiency was not obtained for the range of test conditions covered.

Lewis Research Center,
National Aeronautics and Space Administration,
Cleveland, Ohio, June 18, 1975,
505-04.

REFERENCES

1. Pratt, W.; Leto, A.; and Schaefer, R.: Integral Lift Engine Preliminary Design. (CW-WR-71-091F, Curtiss-Wright Corp.; NAS 3-14327.) NASA CR-120838, 1971.

2. Horlock, J. H.: Axial Flow Turbines; Fluid Mechanics and Thermodynamics. Figure 3.37, Butterworth, Inc., 1966.

3. Stewart, Warner L.; and Glassman, Arthur J.: Analysis of Fan-Turbine Efficiency Characteristics in Terms of Size and Stage Number. NASA TM X-1581, 1968.

4. Zweifel, O.: Spacing of Turbo-Machine Blading, Especially With Large Angular Deflection. Engineering Digest, vol. 3, no. 11, Nov. 1946, pp. 568-570.

5. Zweifel, O.: Spacing of Turbo-Machine Blading, Especially With Large Angular Deflection. Engineering Digest, vol. 3, no. 12, Dec. 1946, pp. 381-383.

6. Whitney, Warren J.; Szanca, Edward M.; Moffitt, Thomas P.; and Monroe, Daniel E.: Cold-Air Investigation of a Turbine for High-Temperature-Engine Application. I - Turbine Design and Overall Stator Performance. NASA TN D-3751, 1967.

7. Whitney, Warren J.; Schum, Harold J.; and Behning, Frank P.: Cold-Air Investigation of a Turbine for High-Temperature-Engine Application. IV - Two-Stage Turbine Performance. NASA TN D-6960, 1972.

8. Aerodynamic Design of Axial Flow Compressors. Revised, NASA SP-36, 1965.

9. Wolfmeyer, G. W.; and Thomas, M. W.: Highly Loaded Multi-Stage Fan Drive Turbine - Performance of Initial Seven Configurations. NASA CR-2362, 1974.

10. Walker, N. D.; and Thomas, M. W.: Experimental Investigation of a $4\frac{1}{2}$-Stage Turbine With Very High Stage Loading Factor. II - Turbine Performance. NASA CR-2363, 1974.

TABLE I. - PERTINENT FEATURES OF BLADE DESIGN

Blade row	Number of blades	Blade length, ℓ, cm	Blade chord at mean radius, C_m, cm	Solidity at mean radius, C_m/S_m	Aspect ratio, ℓ/C_m	Zweifel loading coefficient at mean radius, Z	Leading edge radius at mean section, cm	Trailing edge radius, cm	Reaction at mean radius, R_x
Prewhirl vanes	80	6.800	2.658	1.359	2.56	0.570	0.013	0.013	0.267
Stator 1	55	9.55	5.222	1.836	1.83	.780	.102	.063	.176
Rotor 1	97	10.500	2.898	1.797	3.62	.901	.063	.038	.416
Stator 2	109	11.890	3.096	2.157	3.84	.799	.051	.038	.367
Rotor 2	97	13.172	2.898	1.797	4.54	.901	.063	.038	.416
Stator 3	109	14.986	3.096	2.157	4.84	.799	.051	.038	.367
Rotor 3	99	16.749	2.898	1.797	5.78	.901	.063	.038	.416
Outlet turning vanes	69	16.749	2.883	1.272	5.81	———	.013	.013	-.576

TABLE II. - TURBINE BLADE COORDINATES

(a) Prewhirl vanes

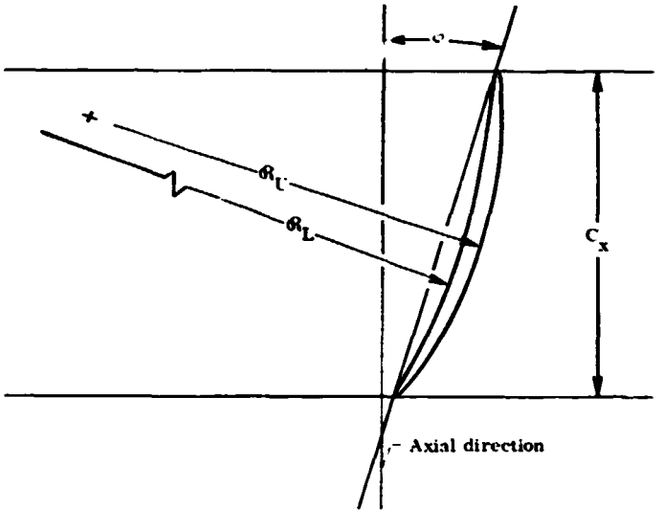

Section radius, cm	Leading edge diameter, cm	Trailing edge diameter, cm	Axial chord, C_x, cm	$\mathcal{R}_L$, cm	$\mathcal{R}_U$, cm	Maximum thickness at midchord, cm	Orientation angle, σ, deg
21.501	0.025	0.025	2.565	6.025	3.663	0.127	17.33
24.901	.025	.025	2.565	7.130	3.993	.127	15.16
28.301	.025	.025	2.565	8.684	4.308	.127	13.37

TABLE II - Continued.

(b) First-stage stator

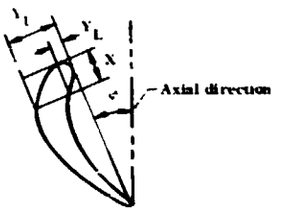

X, cm	Hub		Mean		Tip	
	Section radius, cm					
	20.127		24.901		29.675	
	Orientation angle, ϕ, deg					
	25.20		22.35		20.25	
	Y_L, cm	Y_U, cm	Y_L, cm	Y_U, cm	Y_L, cm	Y_U, cm
0	0.102	0.102	0.102	0.102	0.102	0.102
.102	0	.284	0	.257	0	.241
.305	.130	.551	.114	.472	.094	.424
.508	.272	.770	.239	.663	.198	.592
.711	.386	.945	.345	.831	.297	.739
.915	.478	1.069	.434	168	.389	.874
1.118	.544	1.151	505	1.077	470	.988
1.321	.582	1 201	.564	1 163	.541	1.085
1.524	.622	1.227	.607	1.229	602	1.163
1.727	.638	1.232	.638	1 275	.655	1.227
1.931	.640	1.217	.658	1.298	.699	1.273
2 134	.630	1.181	.663	1.303	.734	1.303
2 337	.607	1.128	.658	1.293	.757	1.321
2 540	.577	1 059	.548	1.267	.767	1.323
2.743	.536	.983	.630	1.227	.767	1.313
2.946	.485	897	.602	1 173	.757	1.293
3.150	.427	.808	.572	1.113	.737	1.265
3.353	.356	709	.533	1.041	.749	1.227
3.556	.282	.602	.490	963	.673	1.129
3.759	.206	488	.442	.881	632	1.125
3.962	.127	.361	.394	792	.567	1.064
4 166	043	.229	.330	.699	.541	.998
4.285	.000	.157	-----	-----	-----	-----
4.348	.063	063	-----	-----	-----	-----
4 369	-----	-----	.269	597	.490	.927
4 572	-----	-----	.203	493	439	848
4 775	-----	-----	135	376	384	.767
4 978	-----	-----	064	254	323	.681
5 159	-----	-----	0	140	-----	-----
5.182	-----	-----	-----	-----	.262	587
5 222	-----	-----	063	063	-----	-----
5 385	-----	-----	-----	-----	.201	490
5 588	-----	-----	-----	-----	137	.384
5 791	-----	-----	-----	-----	074	.274
6.027	--- -	-----	-----	-----	0	137
6 091	-----	-----	-----	-----	063	.063

(c) First-stage rotor

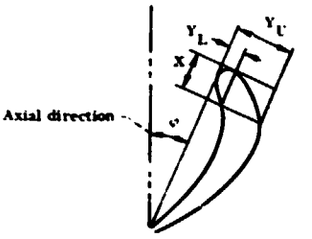

X, cm	Hub		Mean		Tip	
	Section radius, cm					
	19.651		24.901		30.151	
	Orientation angle, ϕ, deg					
	7.23		15.30		23.47	
	Stacking axis coordinates, cm					
	X = 1.285	Y = 0.632	X = 1.270	Y = 0.526	X = 1.321	Y = 0.411
	Y_L, cm	Y_U, cm	Y_L, cm	Y_U, cm	Y_L, cm	Y_U, cm
0	0.048	0.048	0.063	0.063	0.079	0.079
.127	.063	.292	.033	.272	.015	.249
.254	.190	.478	.140	.429	.109	.378
.381	.305	.627	.236	.561	.185	.490
.508	.404	.749	.320	673	.247	.584
.635	.488	.853	.389	.759	.300	.658
.762	.556	.932	.44	.826	.338	.709
889	.607	.991	.485	.871	366	.747
1.016	.648	1.029	.513	.902	.384	.767
1.143	.671	1.049	.531	.912	.391	.772
1.270	.681	1.052	.538	.907	.389	.767
1.397	.676	1.039	.533	.889	.381	.752
1.524	.660	1.011	.518	.858	371	.726
1.651	.630	968	.495	818	.353	.696
1.778	.592	.909	.465	767	.335	.658
1.905	.541	.838	.427	.709	.315	615
2.032	.483	757	384	.645	287	.566
2.159	411	665	.333	.577	259	.515
2.286	.335	566	.279	.500	229	.462
2.413	.251	.460	.221	.422	193	.406
2.540	.162	343	160	.335	155	.345
2 667	074	.213	097	241	114	.271
2.794	-----	-----	030	.142	074	.211
2.817	.038	.038	-----	-----	-----	-----
2 898	-----	-----	.038	.038	-----	-----
2 921	-----	-----	-----	-----	.030	.140
3 053	-----	-----	-----	-----	038	.038

TABLE II - Continued

(d) Second-stage stator

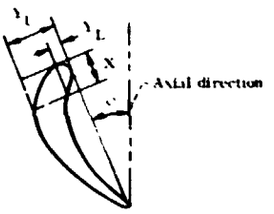

X cm	Hub		Mean		Tip	
	Section radius, cm					
	18.956		24 901		30.846	
	Orientation angle, ϵ, deg					
	14.90		15.35		12 28	
	$Y_{L'}$ cm	$Y_{L'}$ cm	$Y_{L'}$ cm	$Y_{L'}$ cm	$Y_{L'}$ cm	$Y_{L'}$ cm
0	0.051	0.051	0.051	0.051	0.051	0.051
.127	.053	.296	.046	.254	.040	.218
254	.163	.466	.140	409	.117	.340
.381	.254	.597	.221	.538	.185	.446
.508	.326	.695	.287	.648	.248	.538
.635	.378	762	340	737	305	.624
.762	.415	.804	.383	808	.354	698
.889	.436	.824	.417	859	.398	762
1.016	.443	.827	.439	892	.437	818
1.143	.438	.813	.455	.907	.470	.866
1.270	422	.782	.462	912	.497	.904
1.397	.396	.735	.462	.904	517	.932
1.524	.361	.673	.457	886	.533	.950
1.651	320	.599	447	856	.545	958
1.778	.267	.513	.432	818	552	956
1.905	208	.422	.409	775	.554	.947
2.032	140	.318	.387	721	549	931
2 159	064	201	.351	663	.536	907
2.286	-----	076	315	599	518	871
2.306	038	038	-----	-----	-----	-----
2.413	-----	-----	.274	.531	.495	833
2.540	-----	-----	.229	457	.467	787
2 667	-----	-----	178	376	434	.734
2.794	-----	-----	.124	292	398	.678
2 921	-----	-----	.066	198	.357	617
3.048	-----	-----	-----	097	312	552
3.096	-----	-----	.038	038	-----	-----
3 175	-----	-----	-----	-----	267	484
3 302	-----	-----	-----	-----	216	411
3 429	-----	-----	-----	-----	163	334
3 556	-----	-----	-----	-----	107	253
3 683	-----	-----	-----	-----	047	164
3 810	-----	-----	-----	-----	-----	070
3.928	-----	-----	-----	-----	018	038

(e) Second-stage rotor

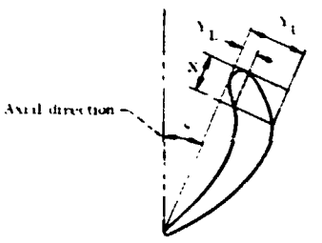

X cm	Hub		Mean		Tip	
	Section radius, cm					
	18.315		24 901		31.487	
	Orientation angle, ϵ, deg					
	5 32		15.30		25 45	
	Stacking axis coordinates, cm					
	X = 1.298	Y 0 665	X = 1 270	Y = 0 526	X = 1 346	Y = 0.284
	$Y_{L'}$ cm	$Y_{L'}$ cm	$Y_{L'}$ cm	$Y_{L'}$ cm	$Y_{L'}$ cm	$Y_{L'}$ cm
0	0.043	0.043	0 063	0.063	0.084	0.084
.127	071	300	033	.272	015	251
254	206	488	140	429	102	371
381	323	637	236	561	173	478
.508	.429	.767	320	673	231	566
635	516	874	389	.459	276	632
.762	584	958	444	526	312	681
889	640	1 024	485	571	335	714
1.016	683	1 064	513	902	.348	732
1.143	709	1.090	531	912	356	737
1.270	719	1.095	538	907	.353	732
1.397	714	1.082	533	889	345	716
1 524	698	1 057	518	858	333	693
1.651	671	1.011	495	818	.320	663
1.778	632	932	465	.767	302	627
1.905	.579	881	427	709	.282	.589
2.032	513	798	384	643	259	546
2.159	437	704	333	577	233	503
2 286	356	597	279	500	208	452
2.413	267	483	221	422	178	401
2 540	170	356	.160	335	145	345
2 667	071	218	097	.241	112	287
2 794	-----	-----	.030	142	076	224
2 807	038	038	-----	-----	-----	-----
2 860	-----	-----	0	086	-----	-----
2 898	-----	-----	038	038	-----	-----
2 921	-----	-----	-----	-----	041	157
3 048	-----	-----	-----	-----	005	086
3.106	-----	-----	-----	-----	038	038

TABLE II - Continued

(f) Third-stage stator

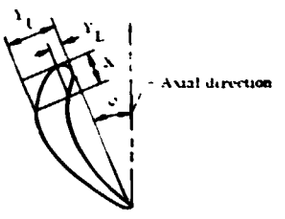

(g) Third-stage rotor

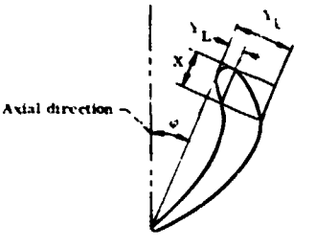

X, cm	Hub		Mean		Tip	
	Section radius, cm					
	17.409		24.901		32.395	
	Orientation angle, φ, deg					
	14.08		15.35		11.32	
	Y_L, cm	Y_U, cm	Y_L, cm	Y_U, cm	Y_L, cm	Y_U, cm
0	0.051	0.051	0.051	0.051	0.051	0.051
.127	.053	.302	.046	254	.036	.201
.254	.170	.472	.140	.409	107	.318
.381	[illegible]	605	.221	.538	.173	.419
.508	.343	.696	287	648	.234	513
.635	394	754	340	.737	.290	.592
.762	.427	787	.383	.806	.343	.666
889	445	.900	.417	.859	.389	.734
1.016	442	.795	.439	892	.432	.790
1.143	.429	.767	.455	907	.467	.841
1.270	.401	.724	.462	912	498	.886
1.397	.363	.658	.462	.904	.526	.919
1.524	.310	.579	.457	.886	.546	.947
1.651	.249	.483	.447	.856	.564	.963
1.778	.178	.378	.432	.818	.577	.970
1.905	.097	.259	.409	.775	.582	.968
2.032	.008	.124	.384	.721	.584	.960
2.096	.038	.038	.368	.693	.582	.955
2.159	-----	-----	.351	.663	.579	.945
2.286	-----	-----	.315	.599	.566	.922
2.413	-----	-----	.274	.531	551	.892
2.540	-----	-----	.229	.457	.528	.851
2.604	-----	-----	.203	.417	.513	.831
2.667	-----	-----	.178	.376	.498	.808
2.794	-----	-----	.124	.292	.465	.757
2.921	-----	-----	066	198	427	.701
3.048	-----	-----	-----	.097	386	.643
3.096	-----	-----	.038	.038	-----	-----
3.175	-----	-----	-----	-----	340	.612
3.302	-----	-----	-----	-----	.292	.513
3.429	-----	-----	-----	-----	.241	.442
3.556	-----	-----	-----	-----	188	.368
3.683	-----	-----	-----	-----	.132	.290
3.810	-----	-----	-----	-----	.074	.206
3.937	-----	-----	-----	-----	-----	117
4.016	-----	-----	-----	-----	.038	038

X, cm	Hub		Mean		Tip	
	Section radius, cm					
	16.526		24.901		33.275	
	Orientation angle, φ, deg					
	3.04		15.30		28.51	
	Stacking axis coordinates, cm					
	X = 1.318	Y = 0.696	X = 1.270	Y = 0.526	X = 1.384	Y = 0.345
	Y_L, cm	Y_U, cm	Y_L, cm	Y_U, cm	Y_L, cm	Y_U, cm
0	0.038	0 038	0.063	0.063	0.089	0.089
.127	.076	.297	033	272	005	251
.254	208	488	.140	.429	.086	363
.381	.333	643	236	.561	155	460
.508	.444	.772	320	.673	211	.536
.635	.538	.889	.389	.759	257	.594
.762	615	980	.444	.826	284	.638
889	.673	1 046	.485	.871	.302	665
1.016	.714	1 097	.513	902	.310	.683
1.143	741	1.128	.531	912	310	.688
1.270	.754	1.139	.538	.907	.305	.683
1.397	.754	1.130	.533	.889	.285	.671
1.524	.742	1.105	.518	.858	.282	.650
1.651	.714	1.062	495	.818	.267	.625
1.778	.673	1.001	.5	.767	.254	.597
1.905	.620	.925	.427	.709	.239	.564
2.032	.554	.838	.384	.645	.221	.528
2.159	.475	742	.333	.577	.203	.488
2.286	.384	.632	279	.500	.183	.447
2.413	.287	.513	.221	.422	.160	.401
2.540	.180	.378	.160	.335	.135	.355
2.667	.069	.226	.097	.241	.109	.305
2.758	0	.104	-----	-----	-----	-----
2.794	-----	-----	.030	.142	.084	.249
2.796	.038	.038	-----	-----	-----	-----
2.860	-----	-----	0	.086	-----	-----
2.898	-----	-----	.038	.038	-----	-----
2.921	-----	-----	-----	-----	.056	193
3.048	-----	-----	-----	-----	.025	.132
3.147	-----	-----	-----	-----	0	.081
3.185	-----	-----	-----	-----	.038	.038

TABLE II. - Continued.

(h) Outlet turning vanes

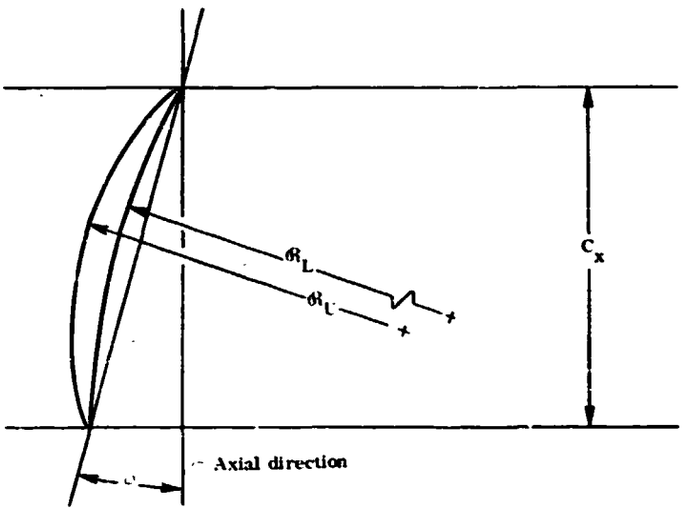

Section radius, cm	Leading edge diameter, cm	Trailing edge diameter, cm	Axial chord, C_x, cm	$\mathcal{R}_L$, cm	$\mathcal{R}_U$, cm	Maximum thickness at midchord, cm	Orientation angle, φ, deg
16.526	0.025	0.025	2.413	3.970	2.080	0.255	19.68
24.901	.025	.025	2.794	6.810	2.748	.274	14.59
33.275	.025	.025	3.175	10.969	3.569	.290	11.41

TABLE II. - Concluded.

(i) Modified first-stage stator

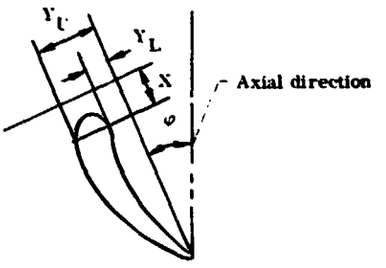

X, cm	Hub		Mean		Tip	
	Section radius, cm					
	20.127		24.901		29.675	
	Orientation angle, φ, deg					
	25.20		22.35		20.25	
	Y_L, cm	Y_U, cm	Y_L, cm	Y_U, cm	Y_L, cm	Y_U, cm
0.538	0.665	0.665	-----	-----	-----	-----
.610	.528	.838	-----	-----	-----	-----
.711	.490	.942	-----	-----	-----	-----
.798	-----	-----	0.711	0.711	-----	-----
.813	.483	1.016	-----	-----	-----	-----
.864	.485	1.046	.579	.879	-----	-----
.914	.493	1.069	.551	.932	-----	-----
1.016	.513	1.115	.531	1.021	-----	-----
1.049	-----	-----	-----	-----	0.765	0.765
1.118	.544	1.151	.531	1.077	.640	.932
1.219	.572	1.181	.544	1.125	.594	1.024
1.321	.592	1.201	.564	1.163	.582	1.085
1.524	.622	1.227	.607	1.229	.602	1.163
(a)	(a)	(a)	(a)	(a)	(a)	(a)
↓	↓	↓	↓	↓	↓	↓
4.348	.063	.063	-----	-----	-----	-----
5.222	-----	-----	.063	.063	-----	-----
6.091	-----	-----	-----	-----	.063	.063

[a]Same as table II(b).

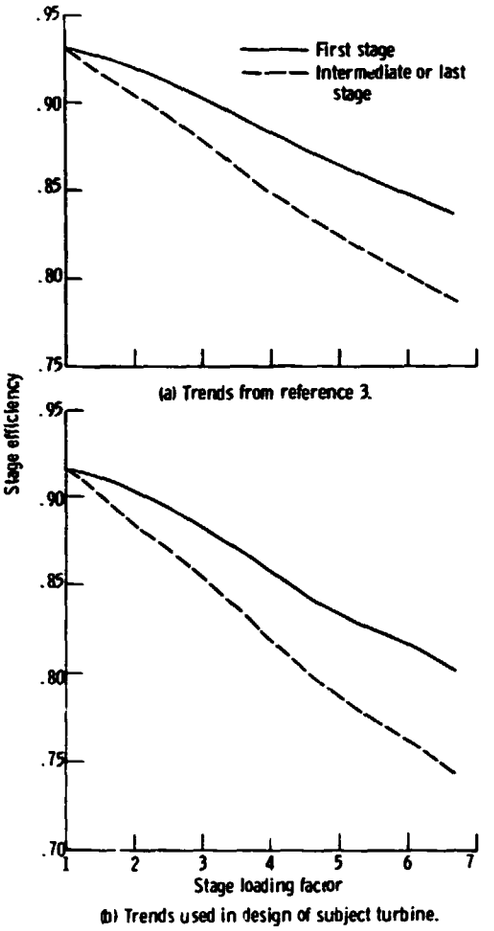

Figure 1. - Comparison of trend of efficiency with stage loading factor from reference 3 with that used in design of subject turbine.

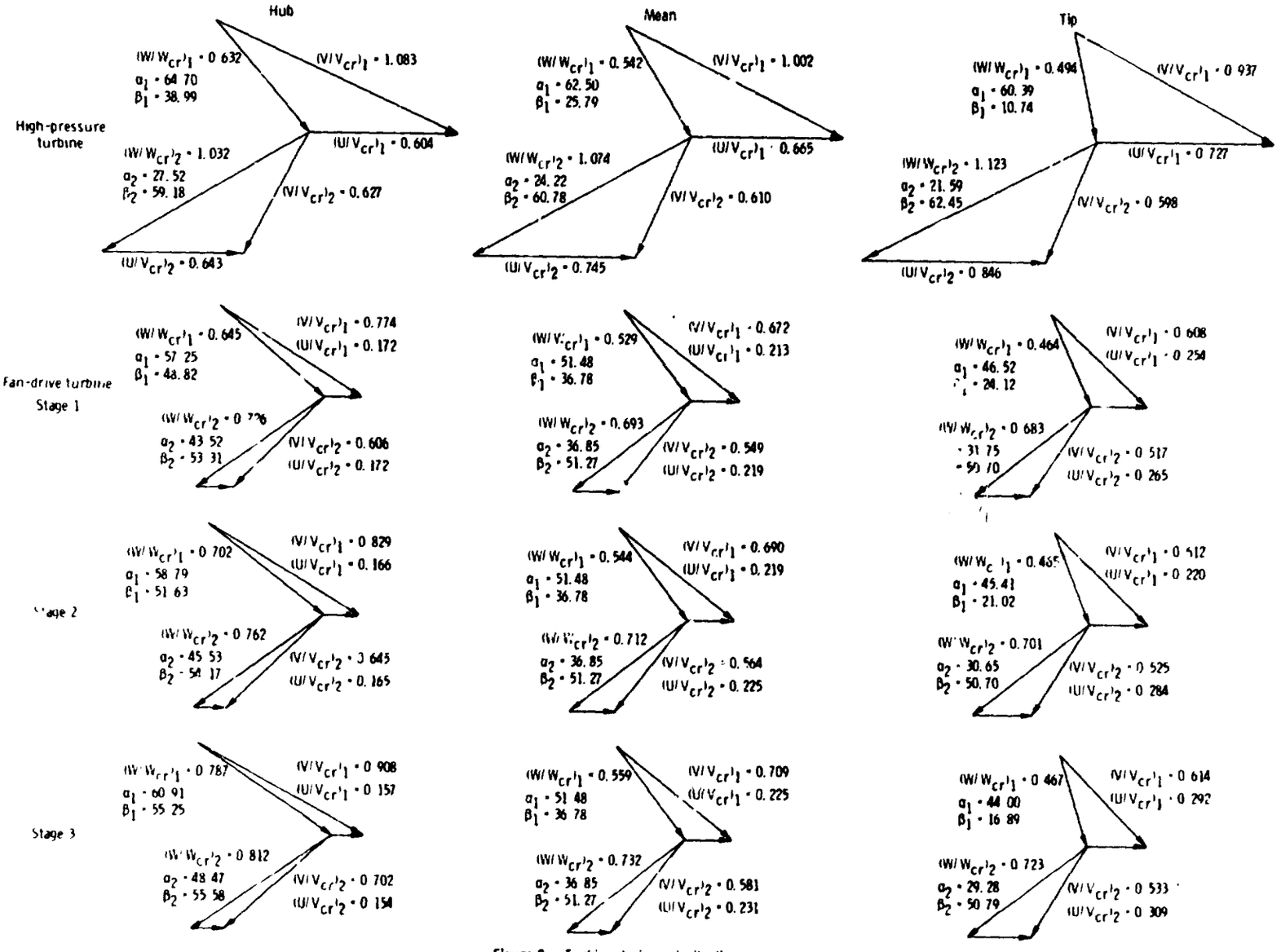

Figure 2. - Turbine design velocity diagrams.

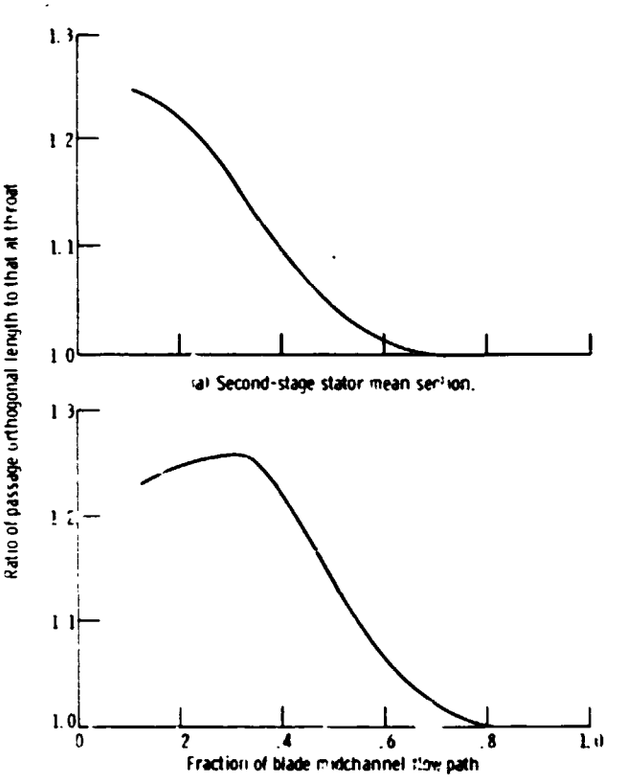

(a) Second-stage stator mean section.

(b) Second-stage rotor mean section.

Figure 3. - Typical blade passage area variations.

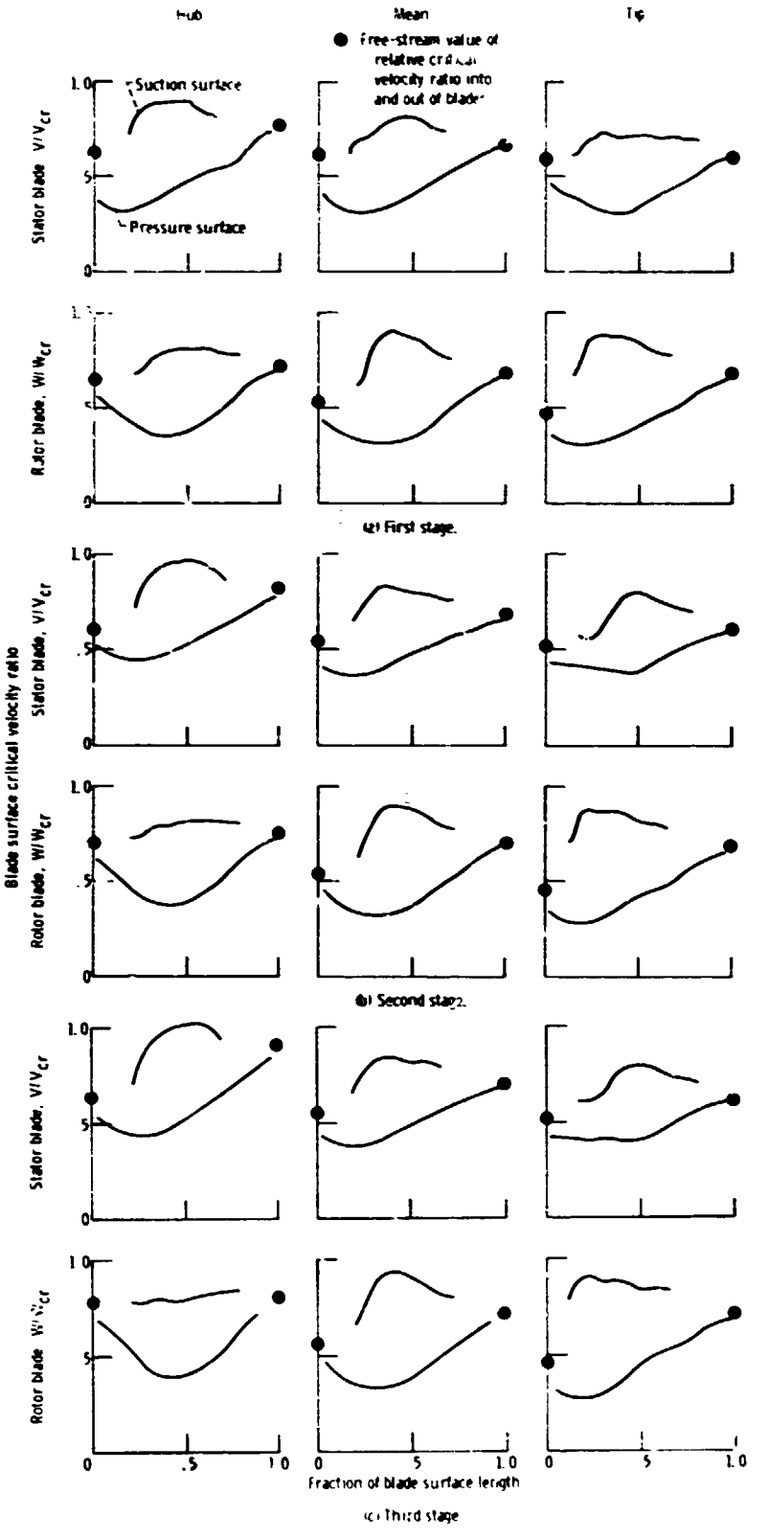

Figure 4. - Design blade surface velocity distributions

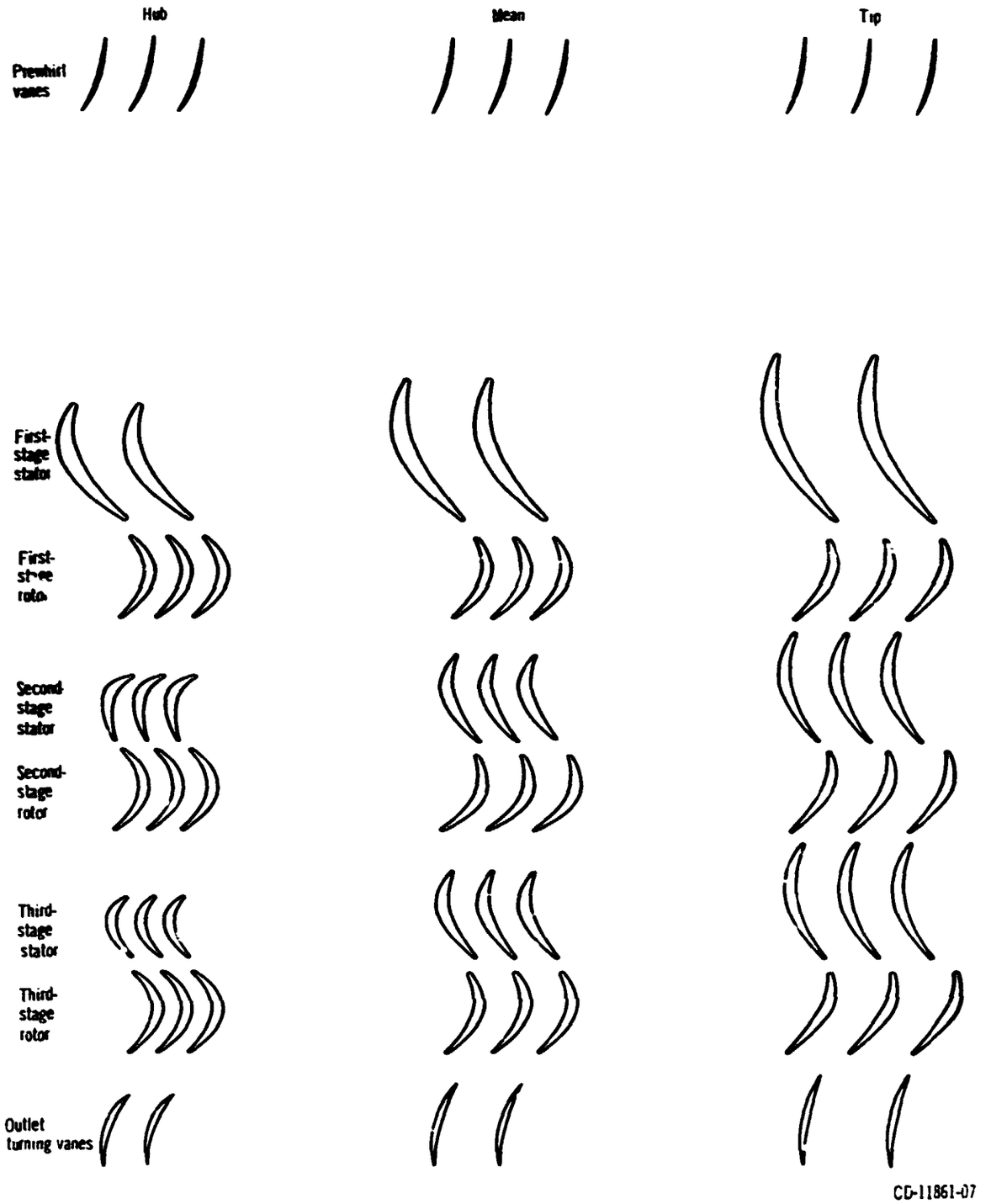

Figure 5. - Schematic of design turbine blading profiles and flow passages.

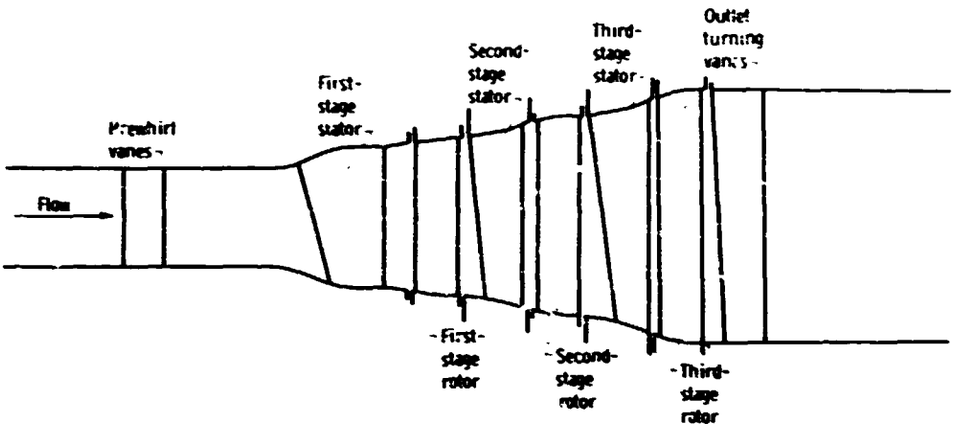

Figure 6. - Flow path through turbine.

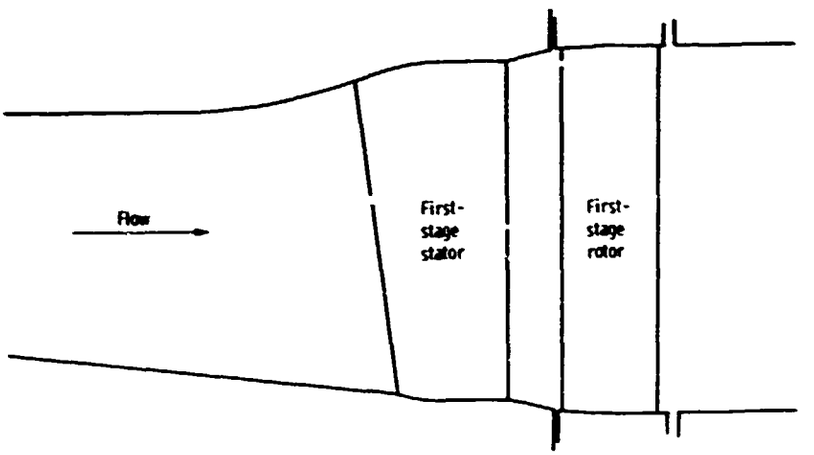

Figure 7. - Flow path through modified single-stage turbine

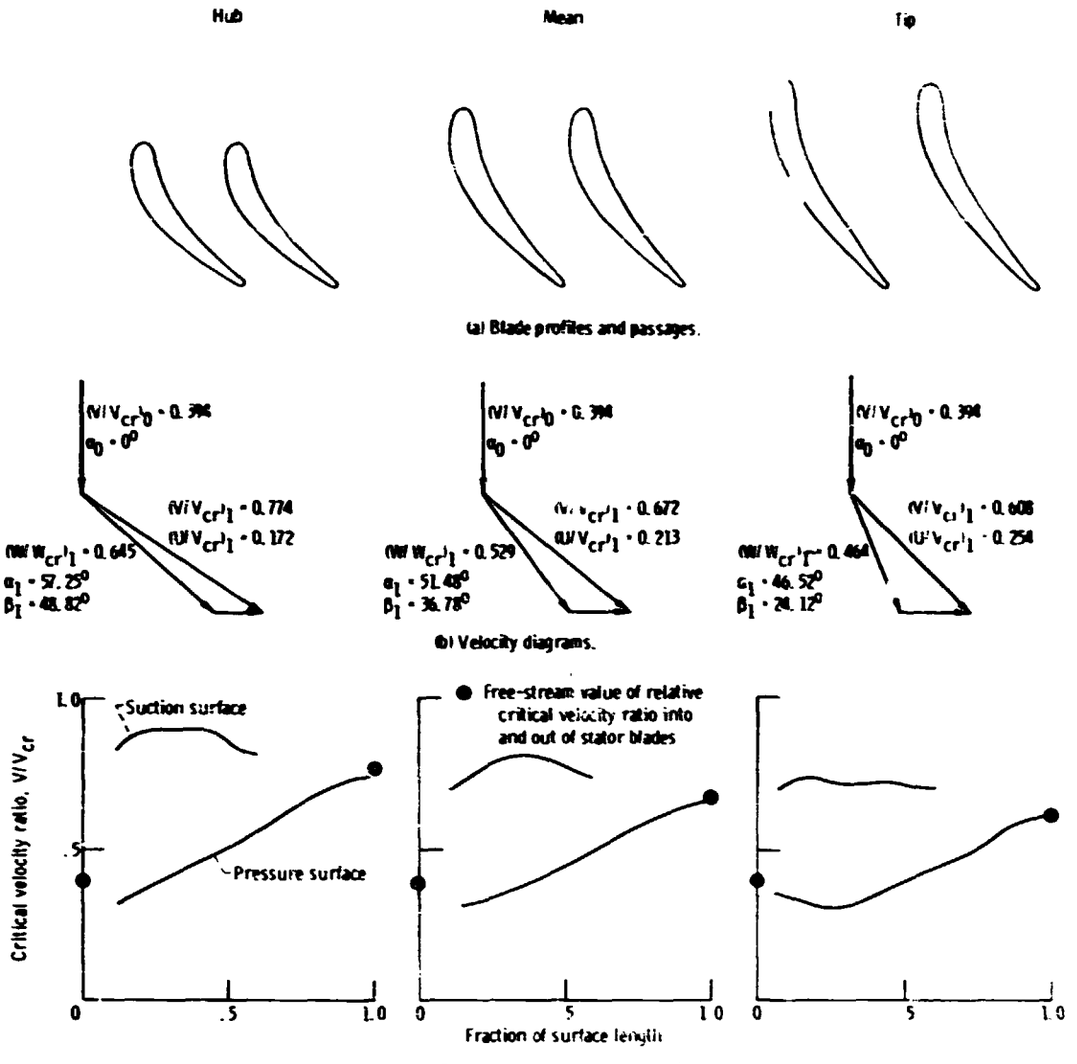

Figure 8. - Modified first-stage stator and design criteria.

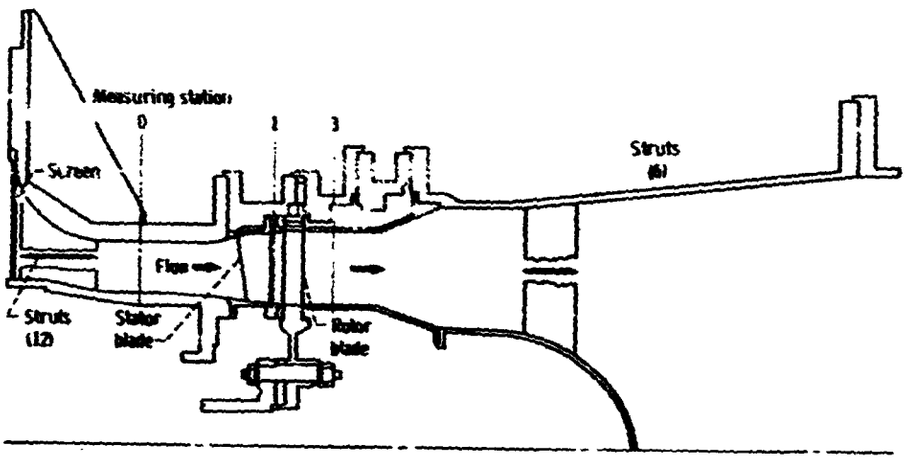

(a) Test section.

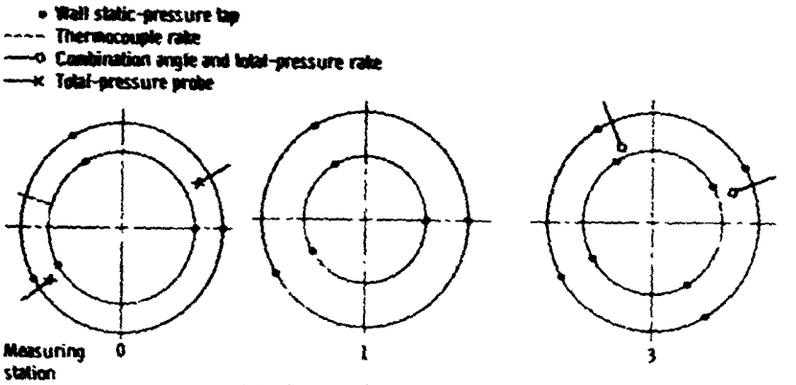

(b) Instrumentation (looking upstream).

Figure 9. - Modified single-stage turbine test section and instrumentation locations.

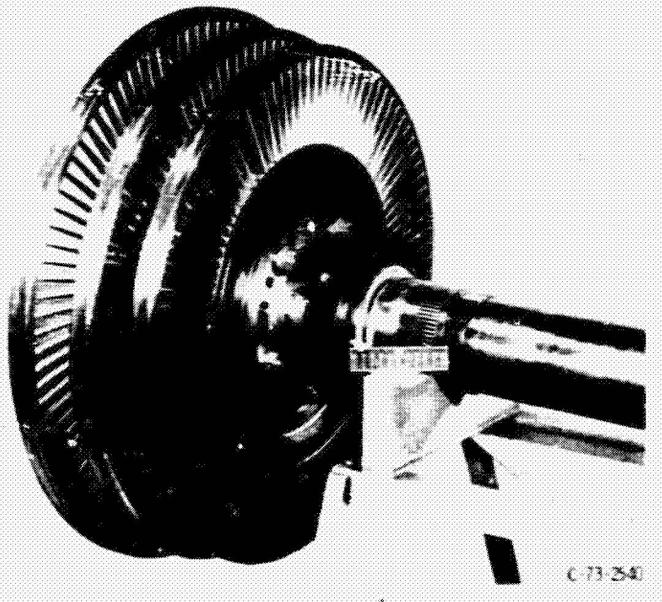

C-73-2540

Figure 10. - Rotor assembly for $3\frac{1}{2}$-stage turbine

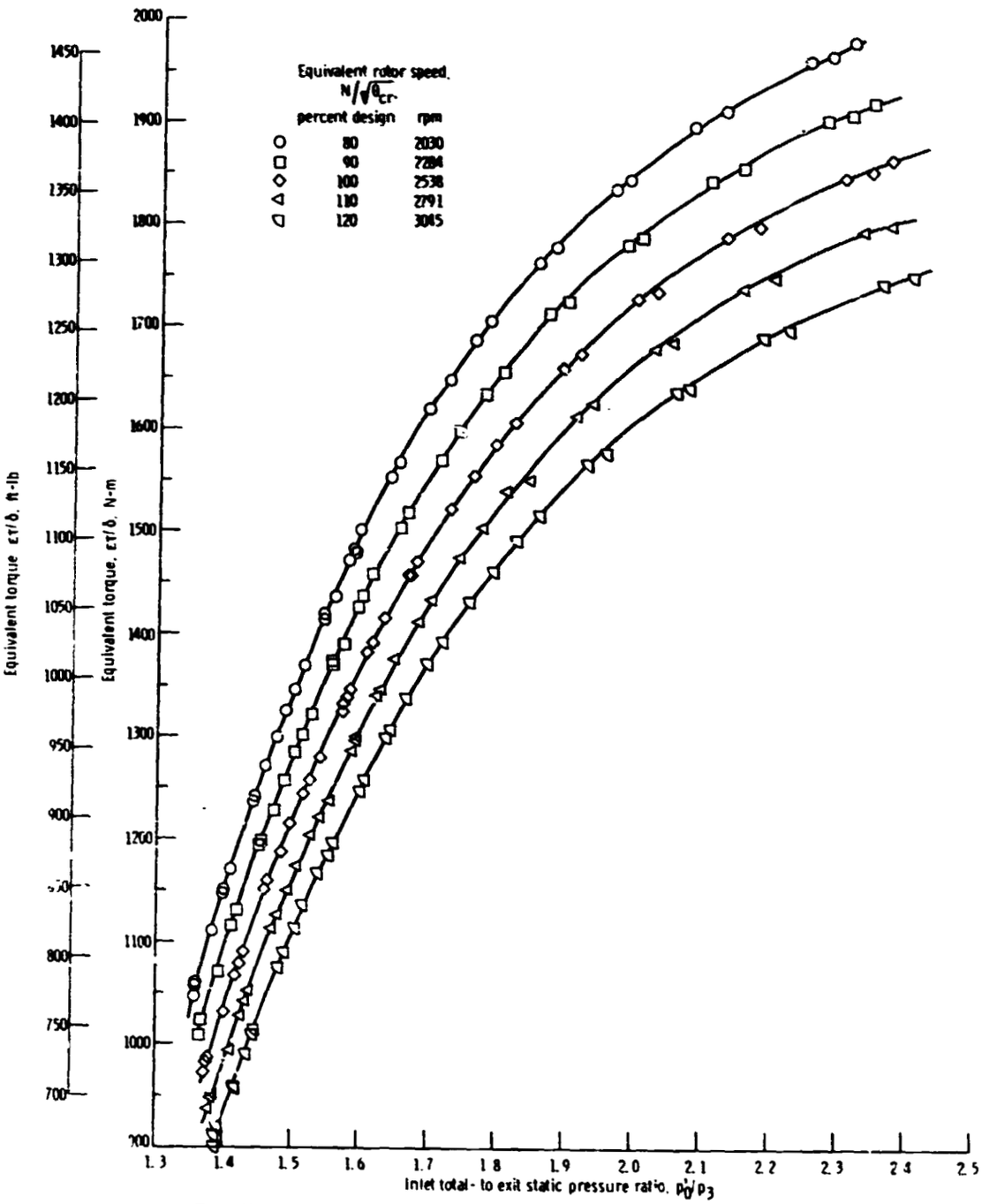

Figure 11. - Variation of equivalent torque with total- to static-pressure ratio for various speeds

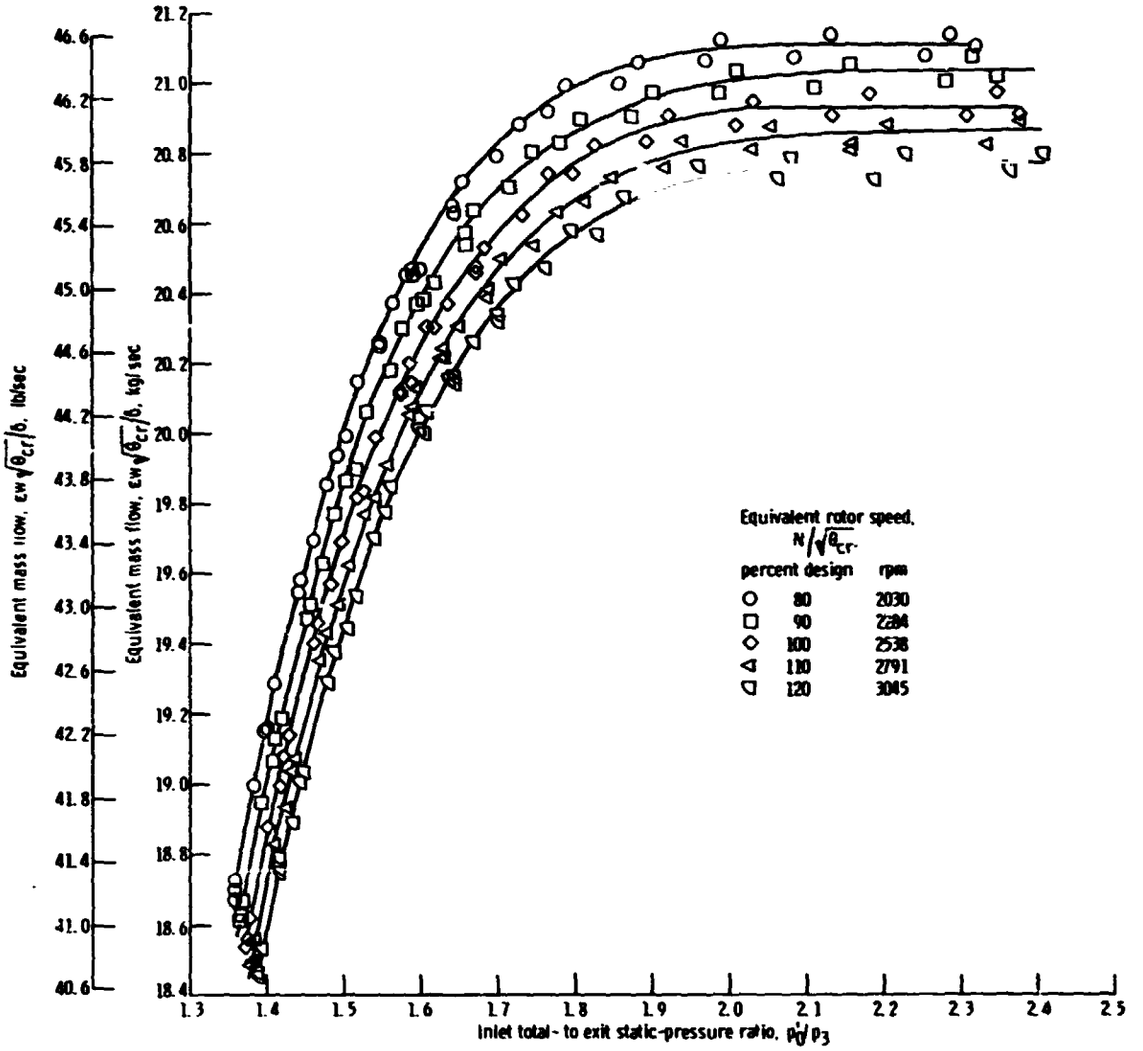

Figure 12. - Variation of equivalent mass flow with total- to static-pressure ratio for various speeds

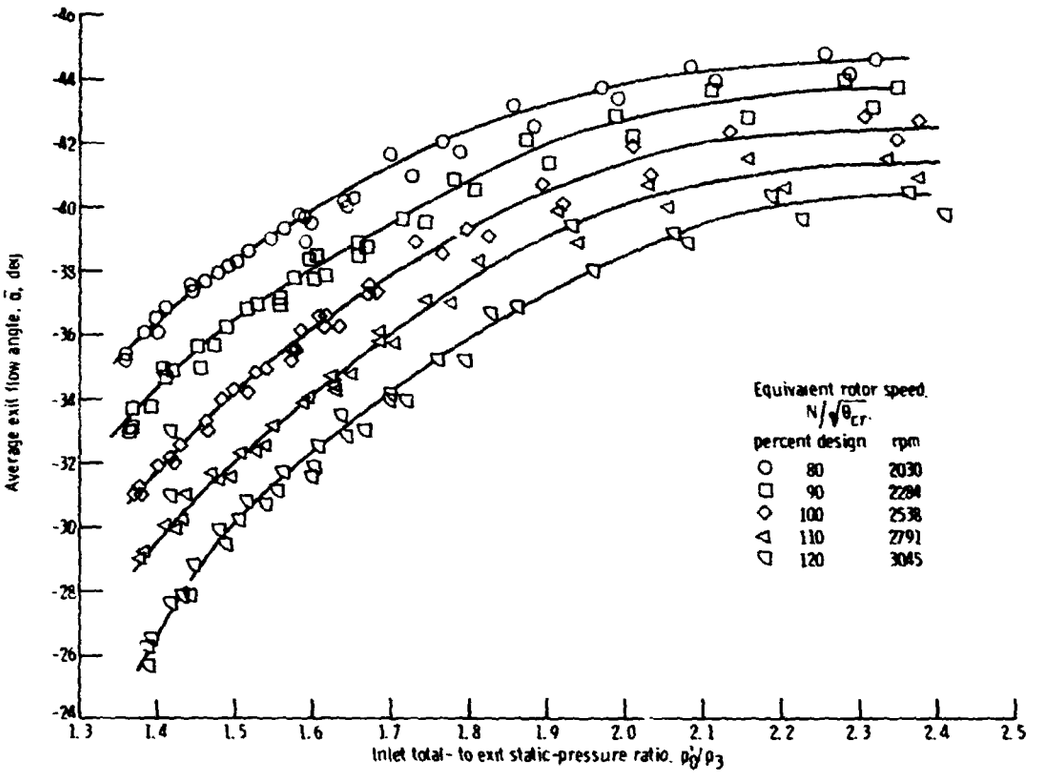

Figure 13. - Variation of average outlet flow angle with total- to static-pressure ratio for various speeds

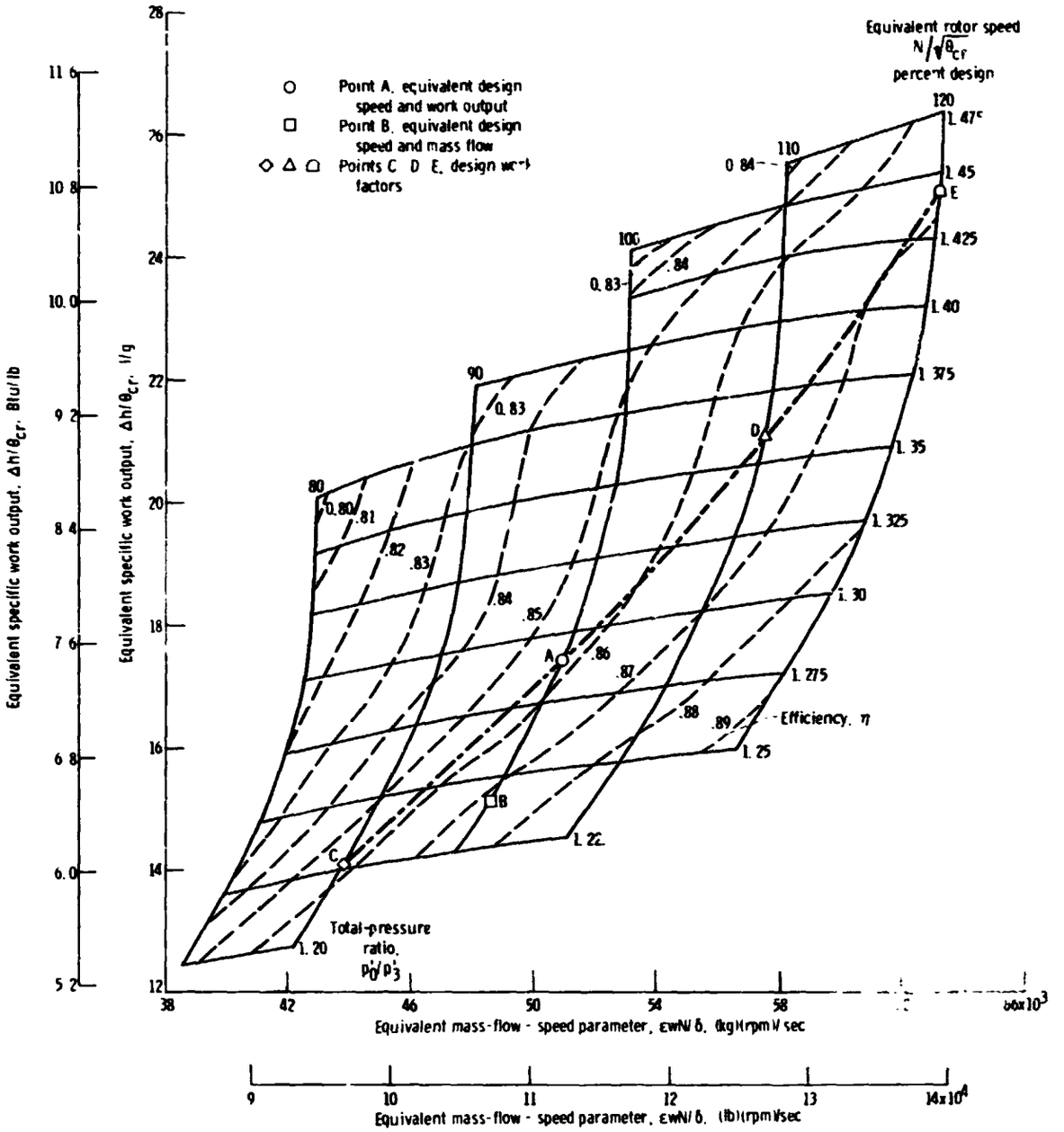

Figure 14. - First-stage performance map.

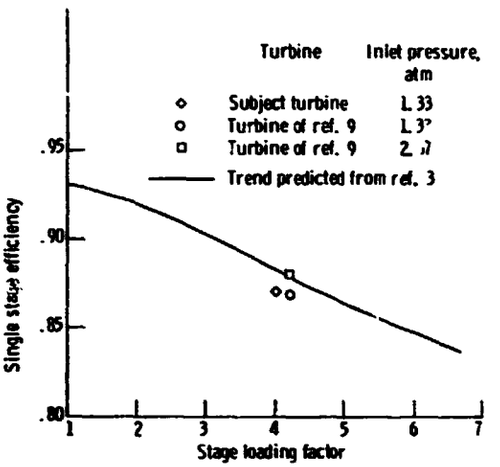

Figure 15. - Comparison of single-stage efficiencies obtained with subject turbine and turbine of reference 9 with efficiency - stage-loading-factor trend predicted by reference 3.

Condition	α_1, deg	β_1, deg	β_2, deg	α_2, deg
Design	51.48	36.78	-51.27	-36.85
Equivalent design work and speed (fig. 16(a))	50.20	35.60	-49.98	-35.52
Equivalent design mass (fig. 16(b))	50.12	33.79	-49.54	-32.50

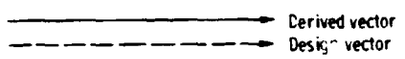

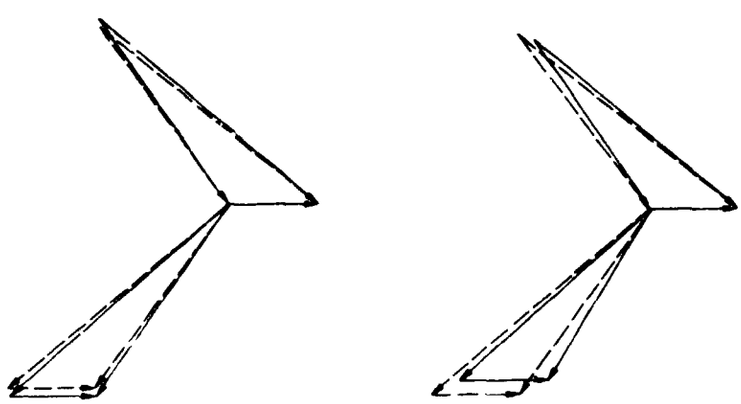

(a) Equivalent design work output and speed (b) Equivalent mass flow and speed

Figure 16. - Comparison of design velocity diagram with that derived from experimental data for points A and B of performance map (fig. 14).